Published by IOP Publishing for Sissa Medialab

Received: *April 3, 2024*
Accepted: *April 23, 2024*
Published: *May 15, 2024*

New studies on the radiopurity and performances of Cs_2ZrCl_6 crystal scintillators

P. Belli[a,b] **R. Bernabei**[a,b,*] **F. Cappella**[c,d] **V. Caracciolo**[a,b] **R. Cerulli**[a,b] **A. Incicchitti**[c,d] **A. Leoncini**[a,b] **V. Merlo**[b] **S.S. Nagorny**[e,f] **V.V. Nahorna**[g] **and P. Wang**[g]

[a] *Dipartimento di Fisica, Università di Roma "Tor Vergata", I-00133 Rome, Italy*
[b] *INFN, Sezione di Roma "Tor Vergata", I-00133 Rome, Italy*
[c] *INFN, Sezione di Roma, I-00185 Rome, Italy*
[d] *Dipartimento di Fisica, Università di Roma "La Sapienza", I-00185 Rome, Italy*
[e] *Department of Physics, Engineering Physics and Astronomy, Queen's University, Kingston, ON, K7L 3N6, Canada*
[f] *Arthur B. McDonald Canadian Astroparticle Physics Research Institute, Kingston, ON, K7L 3N6, Canada*
[g] *Department of Chemistry, Queen's University, Kingston, ON, K7L 3N6, Canada*

E-mail: rita.bernabei@roma2.infn.it

Abstract: In this work, we present new studies by using different materials and procedures to improve the performances and radiopurity of Cs_2ZrCl_6 (CZC) crystal scintillators. In particular, measurements of three new CZC crystals as scintillators were performed over 97.7 days live-time in the low-background DAMA/CRYS set-up deep underground at the Gran Sasso National Laboratory (LNGS) of the I.N.F.N. They allow us to derive elements for improvements towards a possible future use of this kind of detectors in the search for neutrino-less double beta decay of ^{94,96}Zr and rare single beta decay of ^{96}Zr.

Keywords: Double-beta decay detectors; Scintillators, scintillation and light emission processes (solid, gas and liquid scintillators); Gamma detectors (scintillators, CZT, HPGe, HgI etc); Dark Matter detectors (WIMPs, axions, etc.)

*Corresponding author.

https://doi.org/10.1088/1748-0221/19/05/P05037

2024 JINST 19 P05037

Contents

1 Introduction

Over the past few years, a series of articles with a focus on production and studies of Cs_2ZrCl_6 (CZC) luminescent and scintillating properties were published. Firstly, this scintillating compound is attractive as a promising detector to study rare nuclear decays that may occur in natural Zr isotopes, namely neutrino-less double beta decay in ^{94,96}Zr and strongly forbidden single beta decay in ^{96}Zr [1, 2]. Embedding the element of interest into the scintillator material enables a 'source = detector' experimental approach, maximizing the detection efficiency. For instance, in the low-background measurements running over 456.5 days with two CZC crystals of 35 g total mass, experimental limits on different modes of double beta decay in ^{96}Zr were set at level of $T_{1/2} \simeq 10^{17}$–10^{20} yr at 90% C.L. [2]. Secondly, the CZC compound has an extremely high photoluminescence quantum yield to convert deposited excitation energy into scintillation light (close to 70%) [3]; thus, such scintillators are potentially very bright offering an excellent light yield and energy resolution. Indeed, a light yield of about 49400 photons per MeV at room temperature was evaluated with the CZC powder sample in [3]. For the very first produced small-size crystalline sample the light yield was around 25100 photons per MeV [4]; while, the next CZC sample exhibits 33900 photons per MeV [5]. A light yield of about 40900 photons per MeV was recently evaluated for a rather large crystalline sample with dimensions $\varnothing 20\,\text{mm} \times 12\,\text{mm}$ under irradiation by the 662 keV gamma quanta of a ^{137}Cs source [6]. A relatively high light yield results in an energy resolution (FWHM/E) equal to 4.3% at 662 keV and 2.3% at 2.6 MeV. However, there is still room for improvements in the CZC crystal growth methods, raw materials purification and post-growth material treatment, in order to reach a theoretical limit of the material scintillation efficiency. Moreover, in the above mentioned work [2] the first complex study of CZC crystal scintillators in terms of their chemical- and radio-purity was performed. The major contribution to the β/γ background budget was found to be caused by the external gammas from radioactive contamination of the PMTs directly coupled to the CZC crystals. However, the contamination by internal radionuclides also plays a role. For instance, the presence of internal ^{134}Cs cosmogenically activated radionuclide was observed both in measurements of CZC samples with High-Purity Ge gamma-spectrometer, as well as in low-background measurements of CZC's as scintillators [2]. The ^{134}Cs activity at level of 40 mBq/kg comes from the CsCl raw material used

2024 JINST 19 P05037

for the crystal growth. Another background component is caused by internal α active radionuclides from natural U/Th decay chains. It was shown that the main contribution comes from daughters of ^{235}U chain, mainly ^{231}Pa and its progenies with a total activity of about (20–35) mBq/kg [2]. Multi-stage distillation in vacuum of initial $ZrCl_4$ powder appears to be an effective method in the reduction of U/Th concentration down to (0.2–0.4) ppb from their initial values of (70–1000) ppb. However, CZC crystals in previous study were produced from purified $ZrCl_4$ powder with initial chemical purity grade of only 99.9%, which obviously does not satisfy the strict requirement on materials used in low-background experiments. Thus, to reach an ultimate detector radiopurity and experimental sensitivity, raw materials of the highest chemical purity grade processed through additional custom purification should be utilized, and its internal radioactive contamination should be studied in details at each technological stage. As it was highlighted in [7] the higher grade of chemical purity of raw materials leads to a better performance of the detector. Thus, in the present study we will also check this hypothesis in terms of detector scintillation performance and of its internal radiopurity. A recent study [6] showed that the CZC crystals demonstrate an excellent linearity of the light yield for internal electrons (electrons from the Compton scattering of external gamma quanta) in a wide energy range, from 30 keV up to 3 MeV. For the external gamma quanta the linearity is very good down to about 100 keV. Below this energy, a non-proportionality at the level of about (4-6)% is observed. This non-proportionality effect for external excitation could be explained by surface layer degradation. Indeed, when measurements are performed at ambient conditions, environmental humidity in the laboratory may cause the surface layer degradation on a sub-mm-scale. Consequently, non-proportionality will cause a more significant effect on the external low-energy gammas, which are absorbed in a similar mm-scale material thickness. Therefore, it is important to develop an easy and fast method of CZC crystal encapsulation that will prevent surface layer degradation under an ambient humidity and preserve detector performance over a long period of time. In this study we will analyze results obtained with an encapsulation made-of a transparent silicone-based compound.

In this article we present the results obtained with a new development of CZC crystals as room temperature scintillating detectors operating in the DAMA/CRYS setup, a dedicated ultra-low-background facility, located deep underground at Gran Sasso Underground Laboratory (LNGS). The description of these new CZC crystals productions using different materials and procedures, their radioactive contaminations measured by various methods, and their scintillating performances are presented in the various sections. Some considerations to further improve CZC crystals' performances are also discussed in the concluding section.

2 Crystal production

The anhydrous CsCl (99.9%) and $ZrCl_4$ (99.9%), and CsCl (99.999%) and $ZrCl_4$ (99.99%) powders were used as starting materials to produce CZC crystal samples from low and high purity grade reagents, respectively. The two specimens of $ZrCl_4$ powder of both chemical purity grades (99.9% and 99.99%) were subjected to a two-stage sublimation process prior to the Cs_2ZrCl_6 synthesis, see [2] for more details. As-received CsCl and purified $ZrCl_4$ powders of corresponding chemical purity grade were mixed in a stoichiometric ratio, thoroughly grinded in a mortar with a pestle, and loaded in a tapered quartz ampoule with an inner diameter of 22 mm. Then, the mixture was dried by heating at 120 °C for 12 hours under vacuum to remove moisture followed by the reduction stage at 300 °C for 1 hour under the flow of hydrogen. All the Cs_2ZrCl_6 crystals used in this study were grown by

2024 JINST 19 P05037

vertical Bridgman technique. The sealed ampoules with prepared initial reagents were gradually heated and maintained at 850 °C for, at least, 20 hours prior to the growth process in order to form the stoichiometric compound and to ensure the melt homogeneity.

Both crystal boules, CZC-HP (High Purity) and CZC-LP (Low Purity), were produced through two consecutive growth processes — "fast" with a pulling rate of 24 mm/day and a temperature gradient of 20 °C/cm; and a "slow" growth at the pulling rate of 12 mm/day and a temperature gradient of 25 °C/cm. After the latter "slow" growth, the single crystalline boules were cooled-down to room temperature with a temperature gradient of 0.1 °C/min to prevent crystal cracking. Then, crystal boules were cut by a diamond wire saw with mineral oil as a coolant and lubricant. The CZC-HP boule was cut to obtain a single conical sample (⌀(18.0–20.0) mm × 20.0 mm, 19.21 g) from the part of the boule close to the start of the crystallization (nose). Whilst, the CZC-LP boule was cut in the way to obtain two samples – CZC-LP-1 (⌀(18.5–19.5) mm × 20.0 mm, 19.86 g) from the part of the boule close to the start of crystallization, and CZC-LP-2 (⌀19.3 mm × 20.0 mm, 20.43 g) from the middle part of the boule, right after the CZC-LP-1 sample.[1] Furthermore, all the samples were polished with the 1200 grid sand paper using mineral oil as a lubricant. The three CZC samples prepared in the above mentioned manner were thoroughly cleaned by toluene and subjected to encapsulation by using the SYLGARD 184™ Silicone Elastomer Kit. A fused quartz window, placed on the bottom of the mould, was used as optical window and as base that hold (crystal + silicone) composite. After curing the elastomer at room temperature for more than 24 hours, the three samples were extracted from moulds and, without any additional treatment except for wrapping in the light reflecting Teflon tape, were placed in the low-background set-up for long-term measurements.

3 Low background measurements

Each one of the three encapsulated CZC crystals wrapped in foils of Teflon tape was optically coupled to a 3″ ultra-low-background PMTs (HAMAMATSU R6233MOD [9]) in clean environment and placed in the DAMA/CRYS ultra-low-background facility, located deep underground at LNGS in the by-pass between hall A and hall B. The passive shield was made of an innermost layer of 15 cm of OFHC Cu, followed by 20 cm of low-radioactive Pb and by 5 cm of HD polyethylene as external layer. The whole set-up was placed in a Plexiglas box and flushed with high-purity nitrogen gas to reduce radon contribution to the background. Photos of the experimental set-up are shown in figure 1.

The signals from the PMTs were acquired using a CAEN DT5724 14-bit digitizer (100 MSamples/s). An event-by-event data acquisition system recorded scintillating pulses in a time window of 80 µs. No appreciable dead-time is present. The low background data taking started in June 2023 and stopped in October 2023 for a total of 97.7 days.

During the data taking the energy scale and the energy resolution of the three CZC detectors were periodically measured in the same experimental condition as the production runs, by using ^{133}Ba, ^{137}Cs, ^{22}Na, ^{60}Co, ^{226}Ra and ^{228}Th γ sources. As an example, in figure 2 the response of the CZC-HP detector to the ^{137}Cs γ source is shown. Figure 3 shows the linearity (nominal gamma energy vs pulse area) of the energy calibration for the three CZC's, which is very good down to 81 keV (^{133}Ba peak).

[1] The tail part of that boule was discarded to be used as a scintillation detector due to some internal defects.

2024 JINST 19 P05037

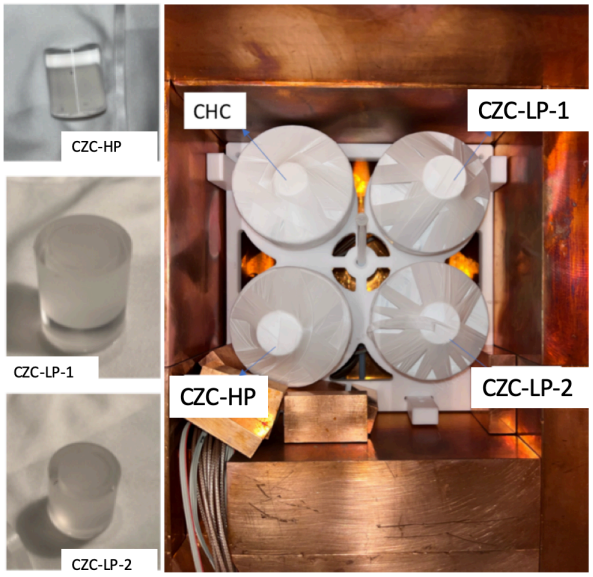

Figure 1. *Left*: pictures of the three CZC crystals encapsulated with SYLGARD 184™ Silicone Elastomer Kit and with fused quartz window. *Right*: the detectors system composed of the three CZC's, during installation. A fourth detector is placed in the system; it is a new Cs_2HfCl_6 (CHC) crystal, not discussed in the present work which is dedicated only to the new developed CZC's.

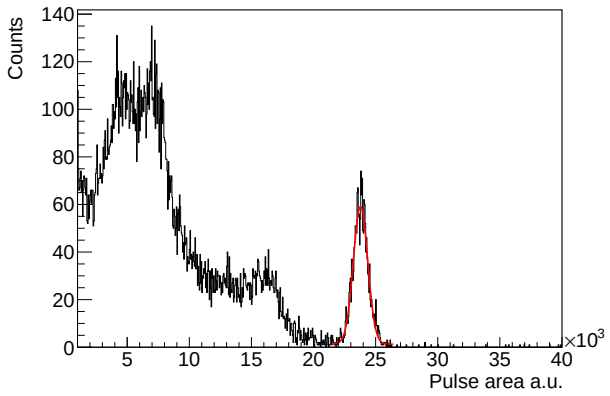

Figure 2. Response of the CZC-HP to a ^{137}Cs gamma (662 keV) source.

The FWHM of each detector (see figure 4) was estimated as $\mathrm{FWHM}_\gamma = \sqrt{p_0 E_\gamma^2 + p_1 E_\gamma + p_2}$ where E_γ, energy of the emitted γ quanta, and FWHM are in keV.[2] The values of the parameters are given in table 1. Thus, for instance, the FWHM was 37 keV (FWHM/E = 5.6%), 40 keV (6.1%), and 44 keV (6.7%) for the 662 keV γ line of the ^{137}Cs source for the three detectors, respectively.

To check the time stability of the energy scale of the three CZC detectors, the data were grouped in time interval of roughly 8-9 days. For each detector the position of a reference peak has been evaluated in each time interval. In particular, the most pronounced peak has been considered for each detector, namely the 662 keV peak in the $\beta(\gamma)$ spectrum of the CZC-HP detector, and the $\simeq$ 1.75 MeV peak in the α spectra of the other two detectors. Figure 5 shows the relative variation of such positions

[2]It should be noted that in this work, when not differently specified, keV means keV electron equivalent.

2024 JINST 19 P05037

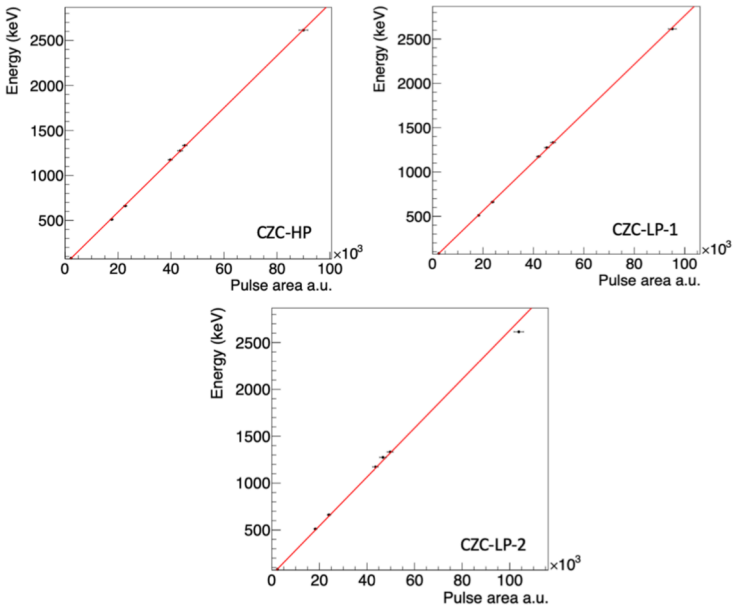

Figure 3. Linearity (nominal gamma energy vs pulse area) of the energy response of the three CZC's measured with γ sources in the energy range (81–2614.5) keV.

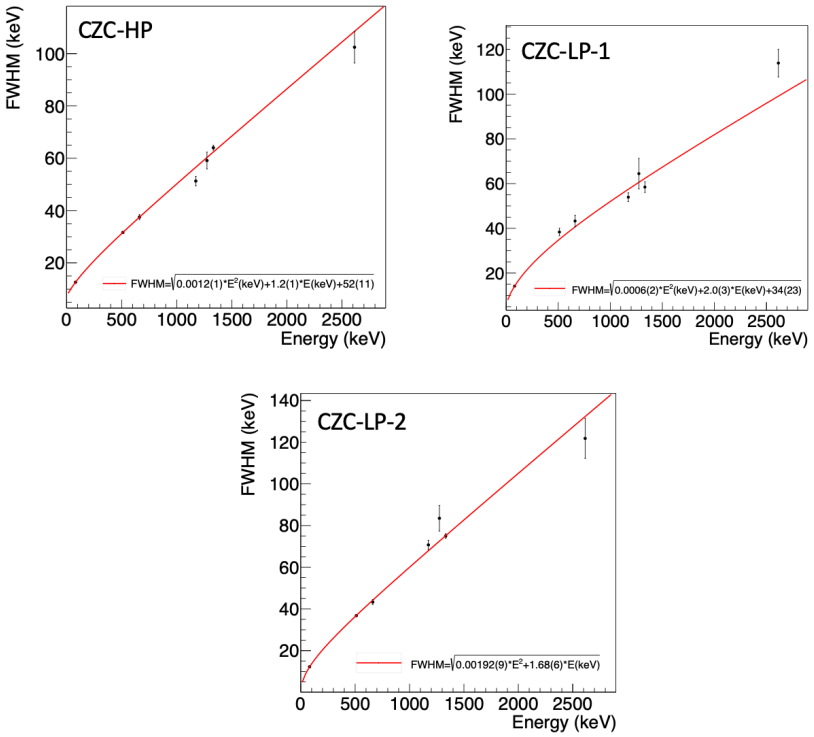

Figure 4. Dependence of the FWHM on the energy for the three CZC detectors. Experimental points were fitted by the function $\mathrm{FWHM}_\gamma = \sqrt{p_0 E_\gamma^2 + p_1 E_\gamma + p_2}$ where E_γ, energy of the emitted γ quanta, and FWHM are in keV. See text.

2024 JINST 19 P05037

Table 1. Values of the parameters obtained in the estimate of the FWHM$_\gamma$ of the three CZC detectors; see text. Note that p_2 is kept null in the fit for the CZC-LP-2 detector; however, when leaving it free, the best fit value is well compatible with zero.

detector	p_0	p_1	p_2
CZC-HP	0.0012(1)	1.2(1)	52(11)
CZC-LP-1	0.0006(2)	2.0(3)	34(23)
CZC-LP-2	0.00192(9)	1.68(6)	0

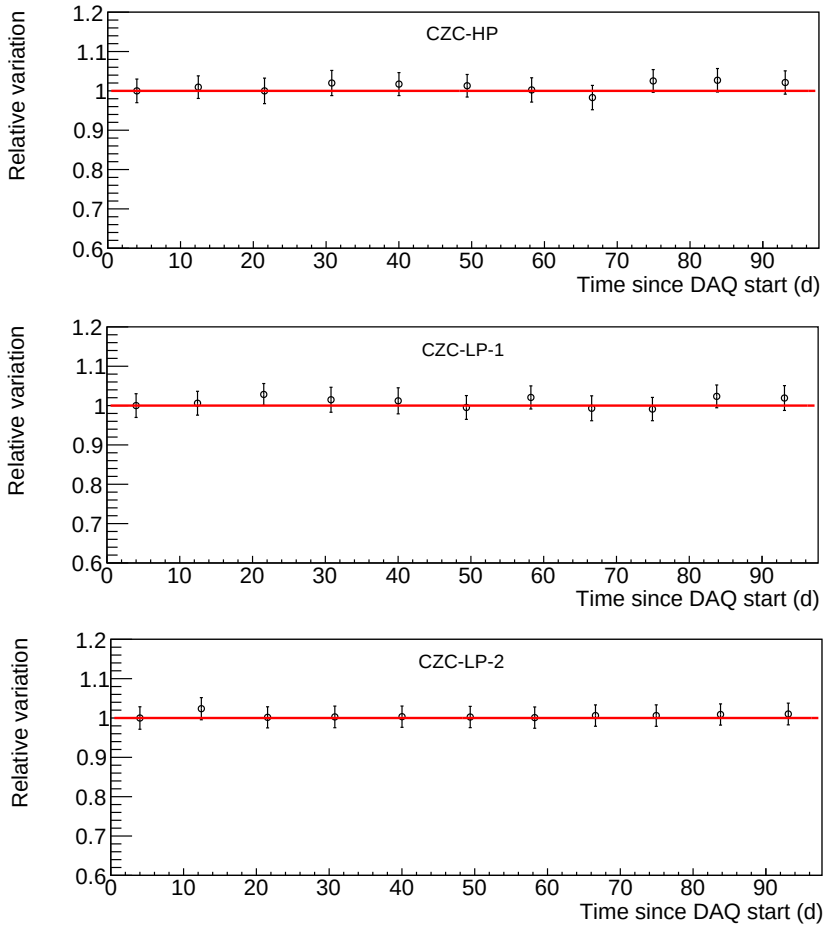

Figure 5. Percentage variation of the position of the reference peaks during the data taking for the three detectors. See text.

as function of time expressed in days. As one can notice, the reference peaks remain rather stable within the experimental errors for all the data taking with a typical variation $< 1\%$.

3.1 Pulse-shape discrimination between $\beta(\gamma)$ and α particles

The pulse-shape discrimination (PSD) technique (based on the investigation of the scintillation pulse mean time; see e.g. [10–12]) was adopted to discriminate $\beta(\gamma)$ events from pulses caused by α-active nuclides in the ^{232}Th, ^{238}U and ^{235}U decay chains internal radioactive contamination in the detectors.

2024 JINST 19 P05037

Typical averaged pulses for α and $\beta(\gamma)$ events were reported in [2]. In particular, the time profile of each scintillation event is exploited to calculate its mean time according to:

$$\langle t \rangle = \sum f(t_k) t_k \Big/ \sum f(t_k), \tag{3.1}$$

where: i) the sum is over the time channels, k, starting from the origin of the pulse up to 24 µs; ii) $f(t)$ is the digitized amplitude (at the time t) of a given signal.

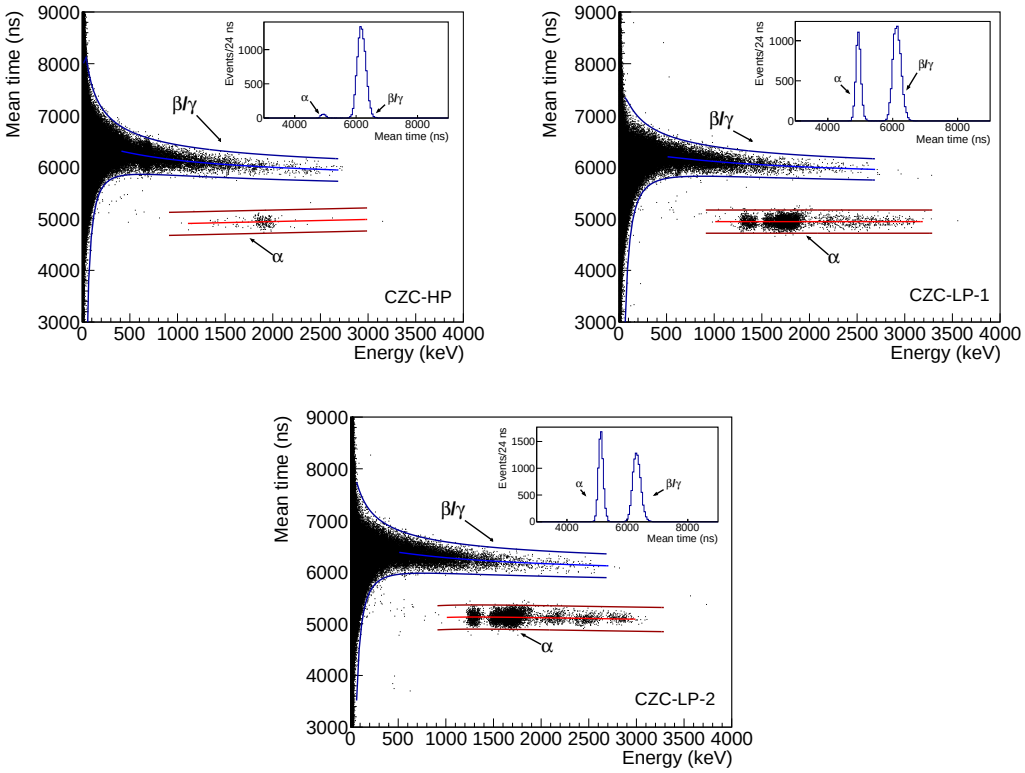

Figure 6. Mean time (see text) versus energy for the low background data accumulated over 97.7 days with the three CZC detectors. The 3σ intervals, around the mean time values, corresponding to $\beta(\gamma)$ and α particles are also shown. Insets: the mean time distributions for events with energies in the range (0.5–3.5) MeV.

The scatter plots of the mean time versus the energy for the data collected by the three CZC detectors are shown in figure 6, together with 3σ intervals. Over the entire energy interval (0.2–3.5) MeV the CZC crystals show an excellent pulse-shape discrimination capability for α particles, i.e. low mean time population, and $\beta(\gamma)$, i.e. high mean time population.

In the α particle population of figure 6, distinct peaks around (1.3–1.8) MeV are observed, attributable to α particles from decays of U/Th chains; further details can be found in section 3.2.

The distributions of the mean time for events with energies in the range (0.5–3.5) MeV are shown in the insets of figure 6. When performing the PSD analysis, one can calculate the figure of merit (FOM), which is related to the goodness of the two peaks separation. It can be determined as:

$$\text{FOM} = \frac{|\mu_\alpha - \mu_\beta|}{\sqrt{\sigma_\alpha^2 + \sigma_\beta^2}}, \tag{3.2}$$

2024 JINST 19 P05037

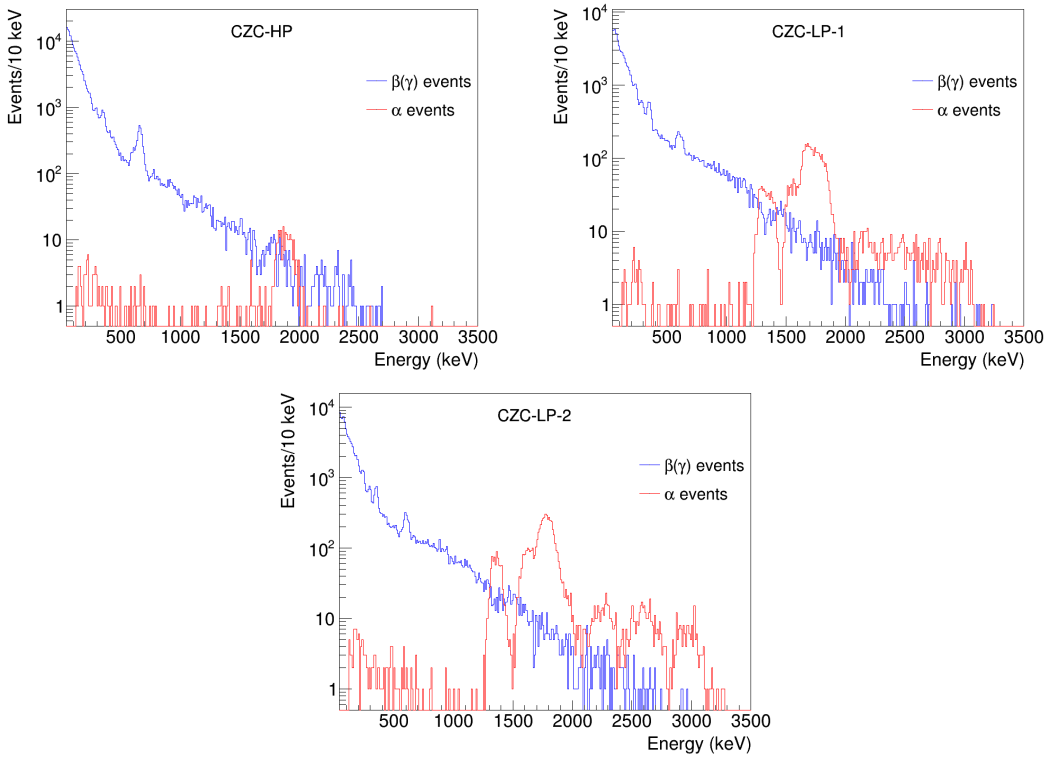

Figure 7. Energy spectra of $\beta(\gamma)$ (blue online) and of α events (red online), measured by the three CZC detectors over 97.7 days live-time of data taking, and identified by PSD (see text).

where μ is the Gaussian mean and σ is the standard deviation of the peaks of α and $\beta(\gamma)$ events in the mean time parameter. In the present case FOM values equal to 8.1, 8.2 and 7.9 have been estimated for CZC-HP, CZC-LP-1 and CZC-LP-2, respectively; these values are averaged in the energy interval (0.5–3.5) MeV.

By applying the PSD selections to events within the 3σ bands shown in figure 6 the energy spectra of "pure" $\beta(\gamma)$ and α events can be obtained. These energy spectra, once corrected for the efficiency of the PSD discrimination (99.7% for α particles and $\beta(\gamma)$ events), are shown in figure 7. In the energy interval (0.04–4.0) MeV the α counting rates, measured over 97.7 days, are: $(173 \pm 10)\alpha$/kg/day, $(2302 \pm 34)\alpha$/kg/day and $(3548 \pm 42)\alpha$/kg/day for CZC-HP, CZC-LP-1, and CZC-LP-2, respectively.

3.2 Study of the α spectra

To estimate the radioactive contaminants in the three CZC crystals, the α spectra (figure 7; red color online) were fitted by a model consisting of α decays from daughter nuclides of ^{235}U, ^{238}U and ^{232}Th decay chains, assuming broken secular equilibrium. Thus, the activities of some nuclides and sub-chains were taken as free parameters of the fit. A factor of efficiency was also considered as a free parameter of the fit for the α peak of ^{215}Po at about 3 MeV (energy in γ scale). The detector energy resolution for α particles and the α/β ratio for α particles with corresponding energies were also introduced into the fit as free parameters.

The background model superimposed to the α spectrum for each detector is shown in figure 8. As regards the CZC-HP detector two background models have been considered: i) the case A where

2024 JINST 19 P05037

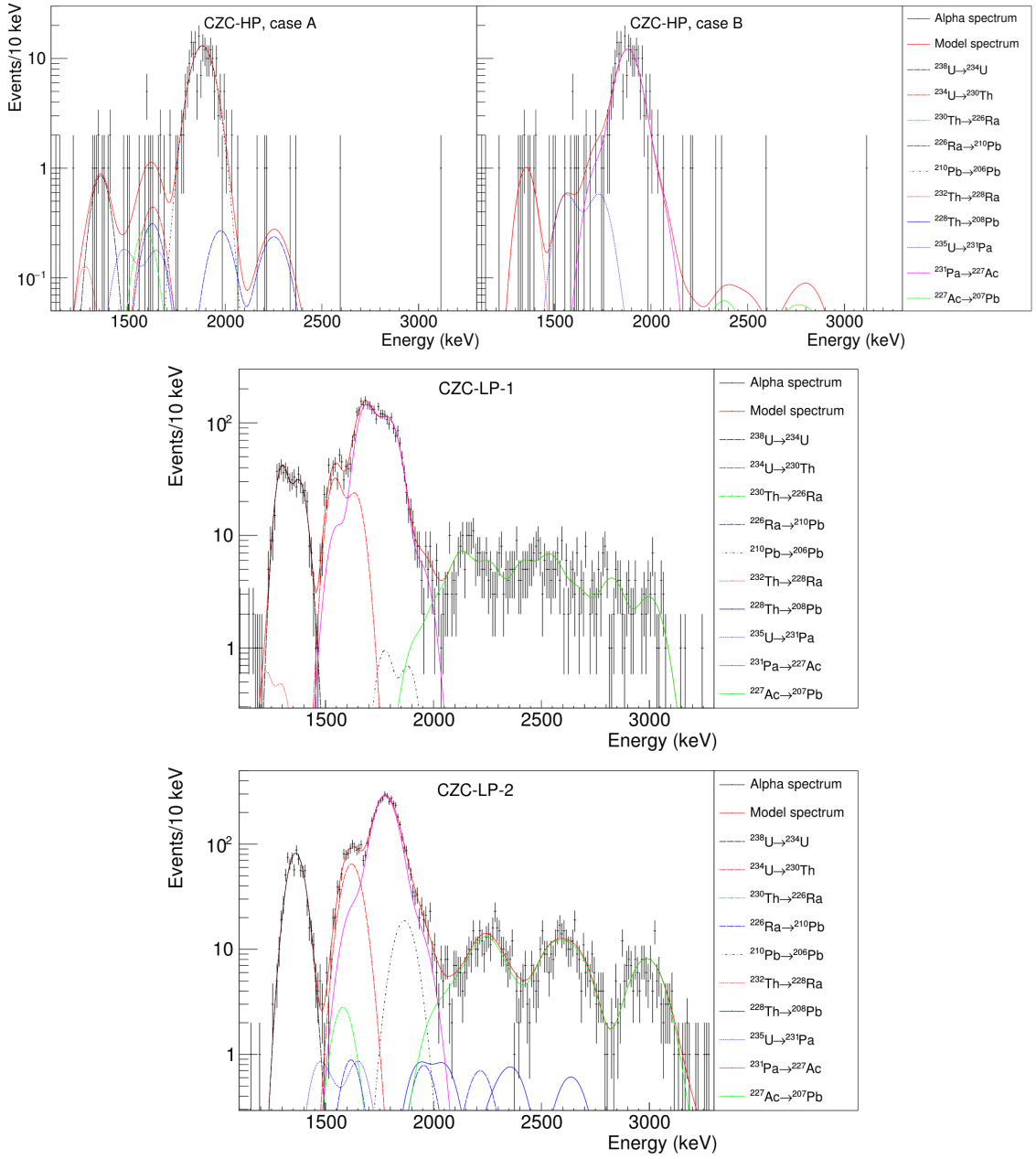

Figure 8. Experimental α spectra (black points) of the three CZC detectors and the background model (red online) considering α decays from ^{238}U, ^{232}Th and ^{235}U chains (colored components online). For CZC-HP two hypotheses are pursued because of the poor number of α events; see text for details.

the main structure is attributed to the ^{210}Po decay (from ^{210}Pb sub-chain; this is also the best fit hypothesis); ii) the case B where the main structure is attributed to ^{231}Pa decay (as also in the other CZC crystals). From the fit one derives $\alpha/\beta = 0.197(18) + 0.0294(34) \times E_\alpha$[MeV] for case A and $\alpha/\beta = 0.220(17) + 0.0285(33) \times E_\alpha$[MeV] for case B; here E_α is the kinetic energy of the α particle. These formulas are valid in the energy interval of the fitting procedure.[3] In particular, the fit of

[3]It should be noted that the value of the α/β ratio depends on many experimental parameters.

2024 JINST 19 P05037

Table 2. Radioactive contaminations of the three CZC detectors derived from the fit of the measured α spectra considering α decays from ^{238}U, ^{232}Th and ^{235}U chains, together with the internal radioactive contamination by ^{40}K, ^{87}Rb, ^{134}Cs and ^{137}Cs derived from the fit of the measured $\beta(\gamma)$ spectra (see section 3.3). The limits are at 90% C.L. "N.D." stands for "not detected" activities.

Chain	Nuclide	Activity, mBq/kg		
		CZC-HP	CZC-LP-1	CZC-LP-2
^{238}U	^{238}U	< 0.08	3.16(14)	4.58(18)
	^{234}U	< 0.12	2.86(22)	4.2(3)
	^{230}Th	< 0.12	< 0.28	< 0.6
	^{226}Ra	< 0.05	< 0.06	< 0.17
	^{210}Pb	< 1.3	< 0.6	1.3(4)
^{235}U	^{235}U	< 0.14	< 0.16	< 0.4
	^{231}Pa	< 1.3	17.0(5)	24.7(6)
	^{227}Ac	< 0.013	0.62(3)	0.94(6)
^{232}Th	^{232}Th	< 0.10	< 0.12	< 0.12
	^{228}Th	< 0.011	< 0.04	< 0.16
	^{137}Cs	100(3)	N.D.	N.D.
	^{134}Cs	58(6)	42(7)	55(7)
	^{87}Rb	1067(5)	318(14)	441(9)
	^{40}K	< 1.1	11(2)	17(3)

the experimental spectrum in the energy interval (1.2–3.2) MeV gives the following χ^2/dof values: 123.6/191 for case A and 151.0/191 for case B. The measured residual contaminations are given in table 2, considering for each nuclide the more cautious limit between the two cases.[4] A 100% efficiency has been adopted for alpha detection to derive the activity values.

For the CZC-LP-1 detector the fit has been performed also adding another gaussian with $E' = 0.942 \times E$ containing about 57% of the events (best fit values); this allows somehow to account for the presence of a double structure which can be ascribed to defects in the crystal. An $\alpha/\beta = 0.2223(28) + 0.02464(59) \times E_\alpha$[MeV] has been measured. The energy spectrum has been fitted in the same energy interval as CZC-HP, obtaining a $\chi^2/dof = 182.0/169$. The measured residual contaminations are also given in table 2.

Finally, the α spectrum of CZC-LP-2 detector has also been fitted in the (1.2–3.2) MeV obtaining a $\chi^2/dof = 228.9/181$, and an $\alpha/\beta = 0.2148(15) + 0.02542(31) \times E_\alpha$[MeV]. The derived residual contaminants are also given in table 2.

In conclusion, the fitting models are in good agreement with the experimental data and have allowed us to derive values on the activities of daughter nuclides from ^{235}U, ^{238}U and ^{232}Th decay chains present as radioactive contaminations in all the three CZC crystals; see table 2.

[4] An upper limit has been derived also for the ^{210}Pb sub-chain in case A and for ^{231}Pa sub-chain in case B, because the origin of the peak at ≈ 1900 keV is not certain.

2024 JINST 19 P05037

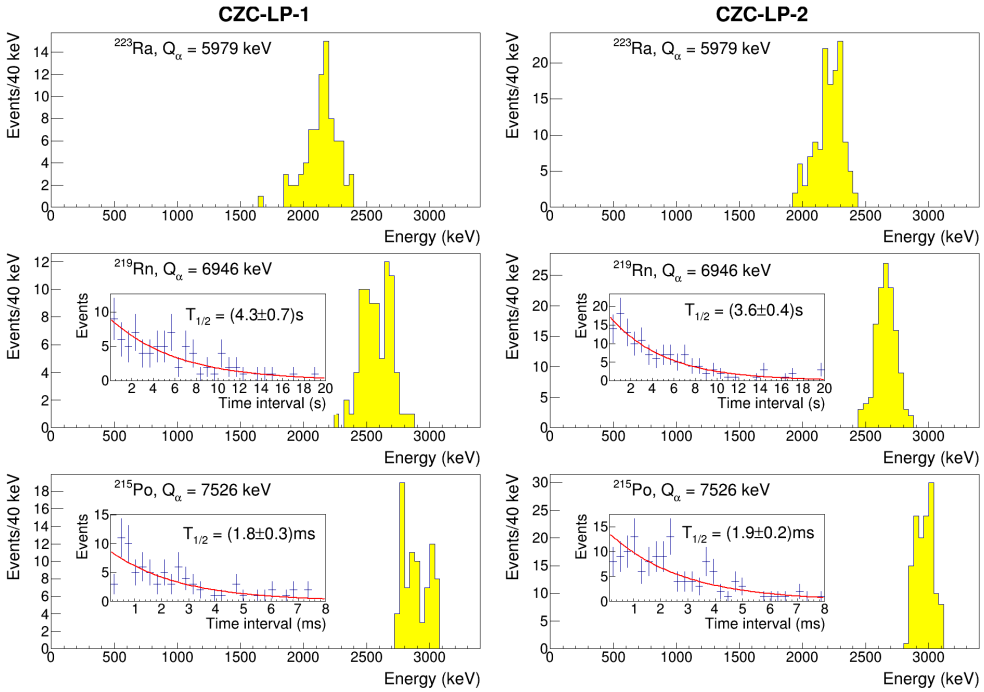

Figure 9. Alpha peaks of ^{223}Ra, ^{219}Rn and ^{215}Po selected by the time-amplitude analysis for the data accumulated with the CZC-LP-1 and CZC-LP-2 detectors. The obtained half-lives of ^{219}Rn and of ^{215}Po are in good agreement with the literature values. Absence of selected events in CZC-HP has allowed us to set just a limit value. See text.

3.2.1 Time-amplitude analysis of ^{235}U contamination

A study has been performed to investigate the origin of the three α structures at higher energy (i.e. E = 2.2, 2.65 and 3.0 MeV in γ scale) by exploiting the time-amplitude analysis. These structures are mostly due to the ^{227}Ac $\rightarrow \ldots \rightarrow$ ^{207}Pb sub-chain from ^{235}U decay chain.

In particular, the arrival time and the energy of each event were used for selecting the fast chain of three α decays in the ^{235}U family: ^{223}Ra (Q_α = 5979 keV; $T_{1/2}$ = 11.44 d) $\rightarrow$ ^{219}Rn (Q_α = 6946 keV; $T_{1/2}$ = 3.96 s) $\rightarrow$ ^{215}Po (Q_α = 7526 keV; $T_{1/2}$ = 1.781 ms) $\rightarrow$ ^{211}Pb. The same energy selection window was used for all the crystals and for all the three α's events in the fast chain: E of α in the range [1500–3800] keV; while for the time intervals between the α's the following values were used: [130 µs–20 s] and [130 µs–8 ms], respectively. The total time intervals efficiency was 87.88%[5], while the total energy windows efficiency was 100%. Figure 9 shows the obtained α peaks and the distributions of the time intervals between events for the CZC-LP-1 and CZC-LP-2 detectors (no events were found for the CZC-HP detector). The half-life of the ^{219}Rn and the ^{215}Po decays resulted to be $T_{1/2}$ = (4.3 ± 0.7) s and $T_{1/2}$ = (1.8 ± 0.3) ms from the CZC-LP-1 data, and $T_{1/2}$ = (3.6 ± 0.4) s and $T_{1/2}$ = (1.9 ± 0.2) ms from the CZC-LP-2 data, respectively. All these values are in very good agreement with those expected from the literature data. Moreover, the fitted peaks positions are well consistent with those obtained by using the α/β ratios previously estimated: they are roughly

[5]This efficiency was evaluated as the product of two efficiencies: i) the first, 96.98%, that the decay of ^{219}Rn occurs in the [130 µs–20 s] time interval; ii) the latter, 90.62%, that the decay of ^{215}Po occurs in the [130 µs–8 ms] time interval. Both are simply calculated considering the exponential decay of such isotopes.

2024 JINST 19 P05037

the same for the two crystals ~ 2200,[6] ~ 2660, and ~ 2980 keV, for the three subsequent α decays respectively. Taking into account the efficiency in the time and energy window to select the ^{223}Ra decay chain, the ^{227}Ac activity in each detector was calculated: 1) CZC-HP: 0 events were found giving rise to the limit value < 0.017 mBq/kg (90% C.L.); 2) CZC-LP-1: 81 events were found giving rise to the value (0.56 ± 0.06) mBq/kg; 3) CZC-LP-2: 132 events were found giving rise to the value (0.88 ± 0.08) mBq/kg. These activities are consistent with those previously obtained in the analyses of the α spectra, shown in table 2.

3.3 Study of the $\beta(\gamma)$ spectra

The $\beta(\gamma)$ spectra of the three CZC crystals (see figure 10) were studied by constructing a background model considering the presence of ^{238}U, ^{232}Th and ^{235}U chains progenitors with their daughters. Radioactive contaminants from the above mentioned chains have been simulated in the crystals and in the various materials of the setup (PMTs, Teflon, Copper). As seen in [9], the PMTs' contribution is dominant compared to the activities measured in the different materials. Moreover, the background model was built also by including internal contaminations from ^{40}K, ^{87}Rb, ^{134}Cs and ^{137}Cs.

The internal contaminations already estimated by the above-reported α analysis were constrained in the fit, leaving them free within $\pm 3\sigma$ around their values (see table 2). In these calculations the EGSnrc code [13] with the DECAY0 event generator [14–16] and — in some cases — a home-made event generator has been adopted. The data have been fitted in the energy interval (200–2700) keV, while a low energy interval has been also considered to determine ^{87}Rb contamination. The corresponding χ^2/dof of the three fits are quite good; in particular, they are: 522.7/441 for CZC-HP, 448.5/443 for CZC-LP-1 and 487.4/432 for CZC-LP-2, respectively.

The obtained contaminations are summarized in table 2.

4 Discussions and conclusions

As seen from the presented results, the encapsulated CZC crystals exhibit excellent scintillation performance stability over the period of the running time (around 100 days). The light yield and energy resolution data collected either within dedicated calibration measurements with external gamma sources, as well as in low background runs, show a great reproducibility and gain stability. Therefore, such an encapsulation method, i.e. using a silicon-based sealant, could be recommended as an easy and fast encapsulation procedure to prevent surface layer degradation and to protect the bulk material of the detectors.

The CZC-HP crystal produced from the higher chemical purity grade CsCl raw material (99.999%) exhibits the higher internal contamination by ^{137}Cs artificial radionuclides (100(3) mBq/kg) with respect to the crystals from the CZC-LP boule (i.e. CZC-LP-1 and CZC-LP-2), produced from CsCl of lower purity grade (99.9%) in which no activity of ^{137}Cs is detected. It can be explained by following. Cesium is produced in an industrial scale by extraction from the pollucite mineral ($Cs_2Al_2Si_4O_{12}\bullet H_2O$) [17]. To extract one kg of Cs salt one needs to use about 100 l of water. In regular extraction process the tap water is utilized without any requirement on its radiopurity. Therefore, the final contamination of a regular CsCl compound is caused by the accumulation of ^{137}Cs present in

[6] This peak is the centroid of the distributions due to several α decays to the excited levels of ^{219}Rn, and considering that the de-excitation γ's are not quenched in the detector.

2024 JINST 19 P05037

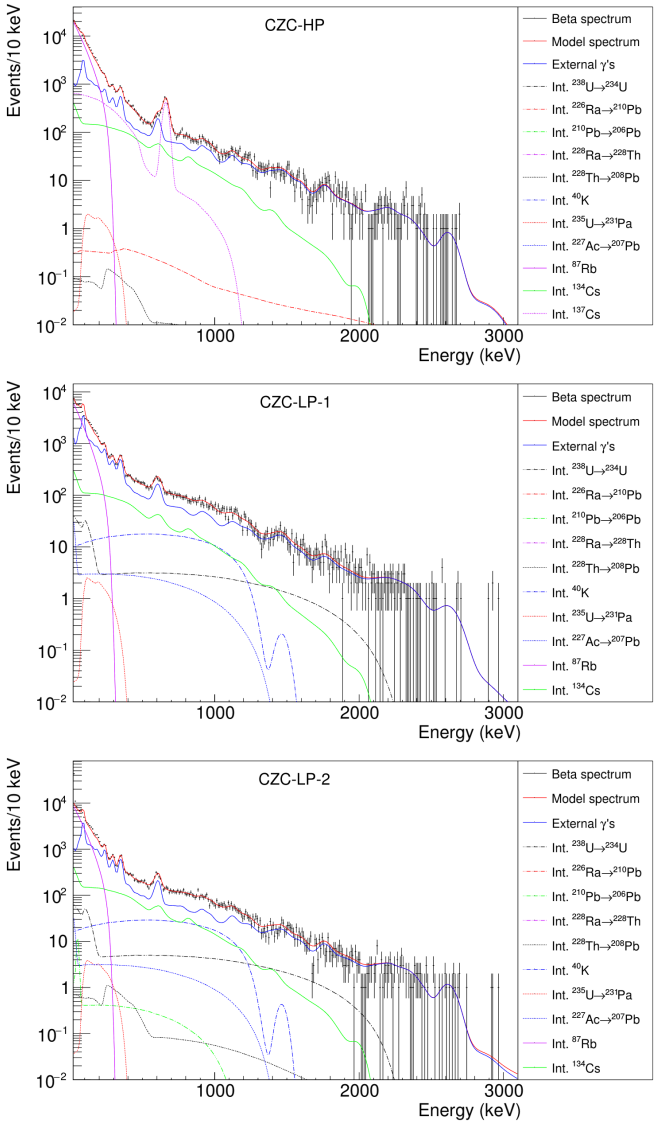

Figure 10. Fit of the $\beta(\gamma)$ spectra of the three CZC detectors considering the internal contamination of ^{238}U, ^{232}Th and ^{235}U chains with their daughters and including contamination by ^{134}Cs, ^{137}Cs, ^{40}K and ^{87}Rb. The "external γ's" wording refers to a cumulative contamination mainly coming from PMTs.

the tap water, being driven by the geographical location of the production site. This contamination could be significantly reduced by using distilled or ultra-pure water as per clean room environment, see [17]. Hence, for the production of low-background CZC crystal scintillators for future experiment, the initial CsCl compound should be extracted and processed only by using ultra-pure water at each technological stage. At the same time, all three CZC samples, regardless of the purity of initial CsCl compound, are contaminated by ^{134}Cs radionuclide at level of about 50 mBq/kg similar to what was observed in earlier studies [2], and confirm the hypothesis of an activation of this nuclide by cosmic rays during CZC samples air transportation to the LNGS site.

Moreover, we have reconsidered the background model of the internal β/γ events including ^{87}Rb β decay instead of ^{135}Cs β decay. Both isotopes decay through pure β decay with released

2024 JINST 19 P05037

energy below 300 keV [18]. In this energy region the energy resolution of our detectors is not enough to distinguish between those two β decays, therefore one should take into account additional independent measurements. Based on the first hint of ^{87}Rb presence in Cs-based detectors [17] and our ICP-MS measurements of CsCl compound (99.9% purity grade), where Rb was detected at the level of 0.7 ppm [19], we have included ^{87}Rb into our background model. More detailed study focused on ^{87}Rb concentration in different materials and its dynamics through crystal growth process is a topic of a separate article that is under preparation. It could also be emphasized that potassium contamination is not detected in high-purity CZC crystal, while is determined in low-purity CZC crystals at a compatible level as in previous study [2]. We can speculate that this represents more effective extraction and purification methods used for high-purity grade CsCl powder production.

In this study we also confirm a previous observation [7, 8]: raw materials of higher chemical purity grade leads to better performances of the detectors, in terms of light yield and energy resolution. For instance, a FWHM/E = 5.6% for the 662 keV gammas of ^{137}Cs was measured with high purity CZC crystal, while FWHM/E = 6.1–6.7% were achieved with low-purity crystal samples of similar mass and sizes. Moreover, the internal contamination by α-active radionuclides is also significantly reduced for high-purity CZC sample with respect to the crystals produced from low-purity raw materials. The internal total alpha activity is lower by a factor 10 or more. Besides, the segregation effect is observed for internal radioactive impurities, confirming previously reported results, see [2]. In the sample cut closer to the tip of the crystalline boule (start of the crystallization process) lower activities were observed for various radionuclides in comparison to the activities in the sample cut closer to the tail of the crystalline boule (end of the crystallization process); see table 2. Hence, several consecutive growing processes using only the first part of the single crystalline boules could be considered as an effective method of CZC crystals purification against daughter radionuclides from U/Th decay chains. In this study we also give detailed analysis of the background model of CZC crystals which is important for developing a new experiment with an enhanced sensitivity in light of searching for neutrino-less double beta decay and rare single beta decay of the ^{96}Zr.

References

[1] E. Celi et al., *New limit on ^{94}Zr double beta decay to the 1st excited state of ^{94}Mo*, *Eur. Phys. J. C* **83** (2023) 396.

[2] P. Belli et al., *Development of low-background Cs_2ZrCl_6 detectors to study rare decays in Zr isotopes*, *Eur. Phys. J. A* **59** (2023) 176.

[3] F. Zhang et al., *Thermally Activated Delayed Fluorescence Zirconium-Based Perovskites for Large-Area and Ultraflexible X-ray Scintillator Screens*, *Adv. Mater.* **34** (2022) 2204801.

[4] K. Saeki et al., *Comparative study of scintillation properties of Cs_2HfCl_6 and Cs_2ZrCl_6*, *Appl. Phys. Express* **9** (2016) 042602.

[5] V. Mykhaylyk et al., *Growth, structure, and temperature dependent emission processes in emerging metal hexachloride scintillators Cs_2HfCl_6 and Cs_2ZrCl_6*, *Dalton Trans.* **51** (2022) 6944.

[6] L. Swiderski et al., *Cs_2ZrCl_6 scintillation properties studied using γ-ray spectroscopy and Compton coincidence technique*, *Nucl. Instrum. Meth. A* **1057** (2023) 168735.

[7] R. Hawrami et al., *Latest Progress on Advanced Bridgman Method-Grown K_2PtCl_6 Cubic Structure Scintillator Crystals*, *IEEE Trans. Nucl. Sci.* **67** (2020) 1020.

2024 JINST 19 P05037

[8] S. Nagorny, *Novel Cs_2HfCl_6 Crystal Scintillator: Recent Progress and Perspectives*, *Physics* **3** (2021) 320.

[9] R. Bernabei et al., *Performances of the new high quantum efficiency PMTs in DAMA/LIBRA*, 2012 *JINST* **7** P03009.

[10] E. Gatti and F. De Martini, *A new linear method of discrimination between elementary particles in scintillation counters*, in *Nuclear Electronics II, Proceedings of the Conference on Nuclear Electronics, Vol. II*, International Atomic Energy Agency (1962), 265–276.

[11] T. Fazzini et al., *Pulse-shape discrimination with $CdWO_4$ crystal scintillators*, *Nucl. Instrum. Meth. A* **410** (1998) 213.

[12] L. Bardelli et al., *Pulse-shape discrimination with $PbWO_4$ crystal scintillators*, *Nucl. Instrum. Meth. A* **584** (2008) 129 [arXiv:0706.2422].

[13] I Kawrakow et al., *The EGSnrc code system: Monte Carlo simulation of electron and photon transport*. Tech. Rep. PIRS-701, National Research Council of Canada, Ottawa, Canada (2003).

[14] O.A. Ponkratenko, V.I. Tretyak and Y.G. Zdesenko, *The event generator DECAY4 for simulation of double beta processes and decay of radioactive nuclei*, *Phys. Atom. Nucl.* **63** (2000) 1282 [nucl-ex/0104018].

[15] V.I. Tretyak, *DECAY0 event generator for initial kinematics of particles in α, β and 2β, decays*, presented at the *French-Ukrainian Workshop*, IJCLab, Orsay, France, 19–23 October 2020.

[16] V.I. Tretyak, in preparation.

[17] Y.D. Kim et al., *Inhibition of ^{137}Cs contamination in cesium iodide*, *Nucl. Instrum. Meth. A* **552** (2005) 456.

[18] R.B. Firestone et al., *Table of isotopes*, 8th Edition, John Wiley & Sons, New York (1996) and CD update (1998).

[19] S. Nisi, private communication.

2024 JINST 19 P05037